

Article

Complexes Between Adamantane Analogues B_4X_6-X = {CH₂, NH, O ; SiH₂, PH, S} - and Dihydrogen, $B_4X_6:nH_2$ ($n = 1-4$)

Josep M. Oliva-Enrich ^{1,*}, Ibon Alkorta ²  and José Elguero ²¹ Instituto de Química-Física “Rocasolano”, CSIC, Serrano, 119, E-28006 Madrid, Spain² Instituto de Química Médica, CSIC, Juan de la Cierva, 3, E-28006 Madrid, Spain; ibon@iqm.csic.es (I.A.); iqmbe17@iqm.csic.es (J.E.)

* Correspondence: j.m.oliva@iqfr.csic.es; Tel.: +34-91-745-95-55; Fax: +34-91-564-24-31

Academic Editors: Igor B. Sivaev, Narayan S. Hosmane and Bohumír Grúner

Received: 6 January 2020; Accepted: 19 February 2020; Published: 26 February 2020



Abstract: In this work, we study the interactions between adamantane-like structures B_4X_6 with $X = \{CH_2, NH, O ; SiH_2, PH, S\}$ and dihydrogen molecules above the Boron atom, with ab initio methods based on perturbation theory (MP2/aug-cc-pVDZ). Molecular electrostatic potentials (MESP) for optimized B_4X_6 systems, optimized geometries, and binding energies are reported for all $B_4X_6:nH_2$ ($n = 1-4$) complexes. All $B_4X_6:nH_2$ ($n = 1-4$) complexes show attractive patterns, with $B_4O_6:nH_2$ systems showing remarkable behavior with larger binding energies and smaller $B \cdots H_2$ distances as compared to the other structures with different X .

Keywords: hydrogen storage; boron; noncovalent interactions; quantum chemistry

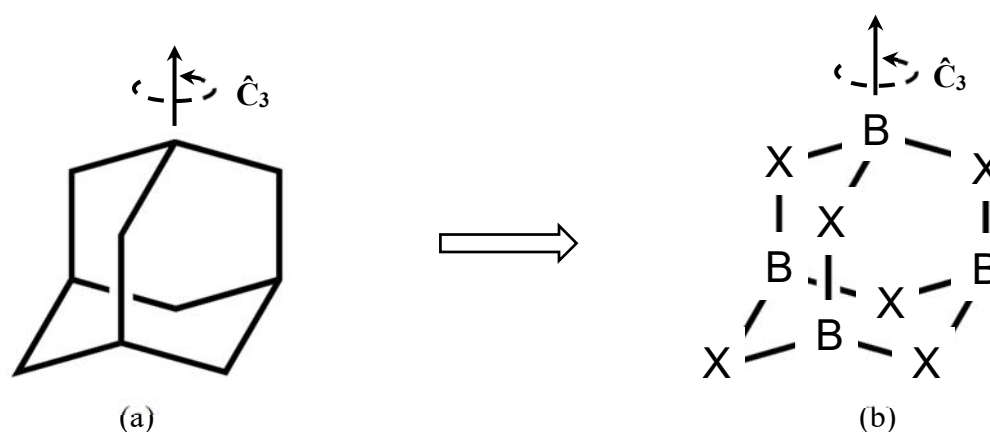
1. Introduction

Hydrogen storage is becoming an important issue regarding the energetic needs of our modern world [1,2]. Different methods are designed for hydrogen storage [3–5], including cryogenics, high pressures, and chemical compounds that reversibly release dihydrogen upon heating [6]. Among the different systems described in the literature, the metal organic frameworks (MOF) have been the most successful ones as hydrogen storage [7–11].

Related to the computational study in the chemical trapping of dihydrogen, noncovalent interactions must be taken into account [12], given the relatively weak attracting force—mostly dispersive—derived from two neutral molecules, leading to general complexes with formula $Z:nH_2$, where Z is a neutral molecule and n is the number of H_2 molecules attached to the Z neutral system. A number of theoretical articles have been devoted to the interaction of dihydrogen with metallic systems [13–22].

The adamantane scaffold is widely used due to their steric [23,24], lipophilic [25] and rigid characteristics [26–30]. Derivatives that include heteroatoms have been synthesized, in addition to the well-known aza-(AZADO and hexamethylenetetramine) [31–34] and oxo-derivatives (tetrodotoxin) [35]. Other derivatives involving C/As/O (arsenicin A) [36], C/N/S (tetramethylenedisulfotetramine) [37], P/S (phosphorus pentasulfide) [38], P/N [39], and C/P/S [40] have also been described.

For the study of dihydrogen complexes, we propose the use of adamantane analog systems where each CH tetrahedral vertex in adamantane is substituted by a Boron atom, and the remaining CH_2 moieties is substituted by divalent X groups, with $X = \{CH_2, NH, O ; SiH_2, PH, S\}$ thus leading to B_4X_6 tetrahedral molecules, as shown in Scheme 1.



Scheme 1. Substitution of CH and CH₂ groups by B and X respectively in (a) adamantane leading to the (b) B₄X₆ systems studied in this work. One of the four equivalent local \hat{C}_3 rotation axis is also shown.

The B₄X₆:*n*H₂ complexes (*n* = 1–4) could be formed by approaching H₂ molecules towards the B atom centered vertically along the four equivalent local \hat{C}_3 rotation axis. The existence of adamantane analogs B₄X₆ is not known, except for the 1-boraadamantane, where only one tetrahedral CH vertex is substituted by a B atom [41], with the remaining structure unaltered; this system has also been the target for a computational study for complex formation [42] with Lewis acids and superacids. Further substitutions of B atoms in tetrahedral sites have been studied from a theoretical point of view only [43]. Directly related to this work is the concept of the, σ -hole, proposed by Politzer and Murray [44–46], which refers to the electron-deficient outer lobe of a *p* orbital involved in a covalent bond, especially when one of the atoms is highly electronegative, that present positive values for the electrostatic potential [47,48]. On the other hand, when the deficient outer lobe of a *p* orbital involved in a covalent bond is perpendicular or axially oriented with respect of the molecular frame, the electrostatic nature of the interactions considered between B atoms in B₄X₆ systems and H₂ molecules can be rationalized in terms of π -holes [49]. We should emphasize the relation between the Lewis acidity of trivalent B centers and the (non)planarity of the structure surrounding the B atom [50].

2. Results and Discussion

2.1. Molecular Electrostatic Potential (MESP) and π -Holes in B₄X₆ Systems

As stated above, we can rationalize the electrostatic nature of the interaction between B₄X₆ and H₂ molecules in terms of π -holes, namely regions of positive electrostatic potential perpendicular or axially-oriented (as in the adamantane structure) with respect to a portion of the molecular framework, as shown in Figure 1. The empty/electron-deficient *p* lobe of Boron pointing outwards in the B₄X₆ systems is an electron (or surplus charge density) attractor, as shown by the positive values of the π -holes.

As shown in Figure 1b, the MESP of the B₄O₆ system shows areas of positive (blue) and negative (red) values corresponding to deficient electron density (negative charge attractor) and surplus electron density (positive charge attractor) areas, respectively. Clearly, the electron density deficiency area above the Boron atoms in B₄X₆ could attract the electron density of the σ bond of the H₂ molecule. As shown in Figure 1b, the large electronegativity of the three oxygen atoms bound to boron must have a stronger effect on the attachment of H₂ molecules as a function of the π -hole values:

$$\pi\text{-hole (au): } 0.131 (\text{O}) \gg 0.058 (\text{NH}) > 0.047 (\text{SiH}_2) > 0.034 (\text{CH}_2) > 0.025 (\text{PH, S}).$$

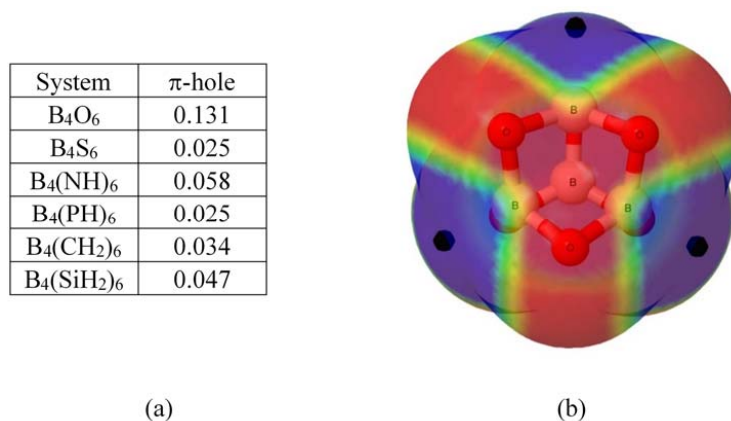


Figure 1. (a) π -hole on the boron atom (a.u.) and (b) molecular electrostatic potential on the 0.001 au electron density isosurface for the B₄O₆ molecule. Red and blue colors indicate Molecular Electrostatic Potential (MESP) values < -0.015 and $> +0.015$ au, respectively. The location of the π -holes is indicated with a black dot.

2.2. Geometries and Energies of B₄X₆:nH₂ Complexes ($n = 1-4$)

Figure 2 shows the optimized geometries of the isolated B₄X₆ systems at MP2/aug-cc-pVDZ level, corresponding to energy minima for all cases. The cartesian coordinates for the B₄X₆ optimized structures are gathered in Table S1, with the MP2 method and basis sets aug-cc-pVDZ and aug-cc-pVTZ, of double- ζ and triple- ζ quality respectively, including diffuse and polarization functions.

In the computations, we first obtain the energy profile of a frozen H₂ molecule approaching this B atom (d distance) along the corresponding local C₃ axis, as shown in Figure 3 for the B₄X₆:H₂ complexes.

From Figure 3 we can clearly observe that all energy profiles are attractive for an H₂ molecule down to 3 Å, and then three different curve patterns emerge: (i) for X = {CH₂, NH, PH, S} the energy profile becomes repulsive when $d < 3$ Å (ii) for X = O, the energy minimum well is flatter and becomes repulsive shifting down to values of $d \sim 1.7-2.0$ Å; and finally (iii) for X = SiH₂ the energy profile remains attractive down to 1.25 Å. The inset plot of Figure 3—upper right corner—shows an energy profile zoom-in of the region $2.5 \text{ \AA} < d < 3.3 \text{ \AA}$ in order to see more clearly the positions of the energy minima regions, for a given X. Clearly, the {CH₂, NH}, and {PH, S} curves show similar energy minima regions: We turn from an attractive to a repulsive system at $d \leq 2.1$ Å (CH₂), 2.2 Å (NH), 2.48 Å (PH), and 2.55 Å (S). As stated above, a zoom-in of the energy profile for $2.5 \text{ \AA} \leq d \leq 3.3 \text{ \AA}$ is included in order to unveil the effect of approaching a H₂ molecule to the B₄X₆ system where several curves have similar profiles. If we observe closely the curves from the zoom-in inset of Figure 3, the energy minima for CH₂, NH, PH, and S are located as follows: $d_{\min}(\text{CH}_2) \sim 2.73$ Å, $d_{\min}(\text{NH}) \sim 2.77$ Å, $d_{\min}(\text{PH}) \sim 3.05$ Å, $d_{\min}(\text{S}) \sim 3.06$ Å. For O and SiH₂ there are no minima within this region since the curves are always attractive.

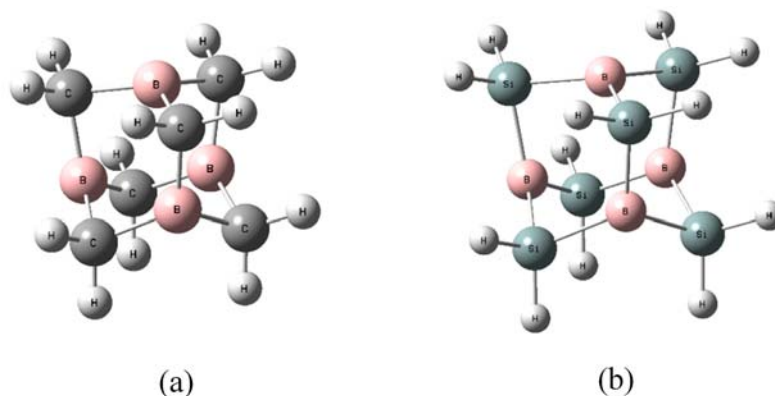


Figure 2. Cont.

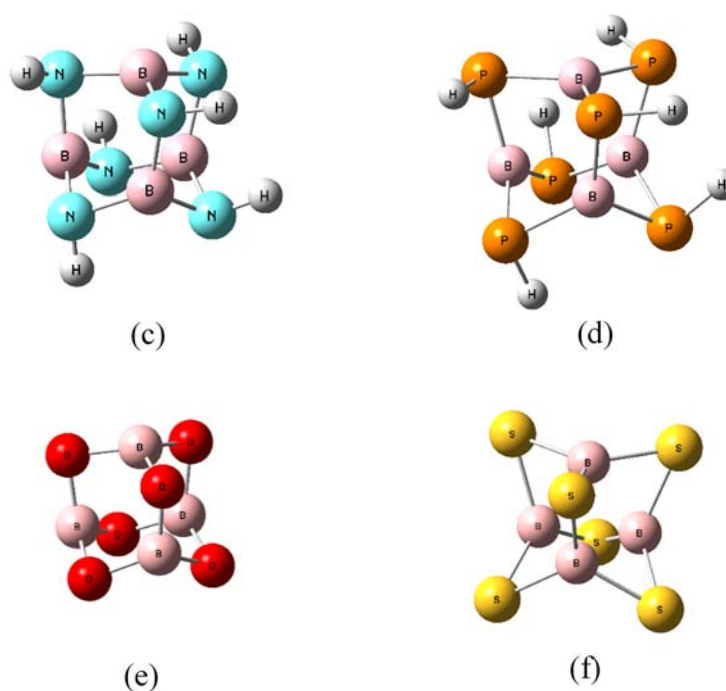


Figure 2. MP2/aug-cc-pVDZ optimized geometries of adamantane-like B_4X_6 systems, (a) $X = CH_2$, (b) $X = SiH_2$, (c) $X = NH$, (d) $X = PH$, (e) $X = O$, (f) $X = S$. All geometries correspond to energy minima. Cartesian coordinates gathered in Table S1.

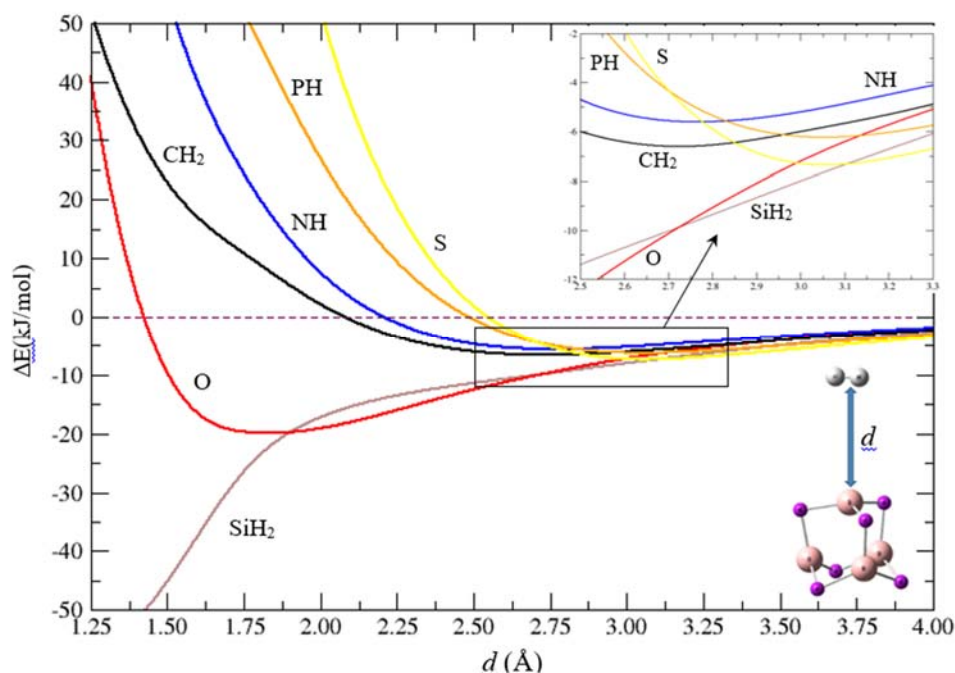


Figure 3. Energy profiles of $\Delta E = E(B_4X_6:H_2) - E(H_2)$, in kJ/mol, versus d , in Ångström, for different X at MP2/aug-cc-pVDZ computational level. The geometries of B_4X_6 and H_2 are kept frozen along the d coordinate. The inset plot on the upper right corner corresponds to a zoom-in region of ΔE versus d within the range $2.5 \leq d \leq 3.3$ Å, showing the corresponding energy minima for CH_2 , NH , PH and S systems.

Once we choose the d which corresponds to the energy minimum in Figure 3, we relax the nuclear coordinates in the whole complexes hence determining the energy minimum structure for the $B_4X_6:nH_2$

systems. Due to the different behavior of the $B_4(SiH_2)_6$ system versus an H_2 molecule—permanent attractive profile for d down to 1.25 Å—as compared to the other complexes—Figure 3—and the lack of an energy minimum geometry for the $B_4(SiH_2)_6:H_2$ complex – a geometry optimization shows a bond breaking in the H_2 molecule and a rearrangement of the $B_4(SiH_2)_6$ adamantane structure—this system will be analyzed further in another work. The optimized structures for all $B_4X_6:nH_2$ complexes ($n = 1-4$) are depicted in Figure S2, except for $B_4O_6:nH_2$ ($n = 1-4$), the latter shown in Figure 4. In Table 1 we gather the average $B\cdots H_2$ and $H\cdots H$ distances in the optimized geometries of the different $B_4X_6:nH_2$ complexes, all corresponding to energy minima at the MP2/aug-cc-pVDZ level of theory.

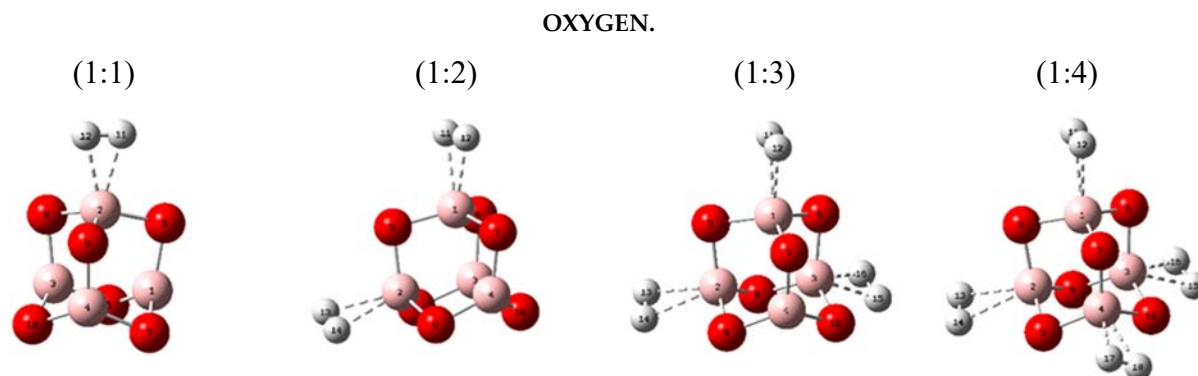


Figure 4. Optimized geometries for the $B_4O_6:nH_2$ complexes ($n = 1-4$) with MP2/aug-cc-pVDZ computations. All geometries correspond to energy minima.

Table 1. Average $B\cdots H_2$ (d) and $H\cdots H$ distances (Å) in the $B_4X_6:nH_2$ complexes, $X = \{CH_2; NH, PH; O, S\}$ with MP2/aug-cc-pVDZ computations. The H-H distance in the isolated H_2 molecule is 0.755 Å, computed at the MP2/aug-cc-pVDZ level of theory.

X	B...H ₂				H-H			
	1:1	1:2	1:3	1:4	1:1	1:2	1:3	1:4
CH ₂	2.737	2.740	2.745	2.750	0.755	0.755	0.754	0.754
NH	2.777	2.727	2.705	2.727	0.755	0.755	0.755	0.755
PH	3.080	3.045	3.046	3.049	0.755	0.755	0.755	0.755
O	1.624	1.687	1.766	1.850	0.774	0.770	0.766	0.763
S	3.071	3.070	3.068	3.068	0.755	0.755	0.755	0.755

As regards to the $B\cdots H_2$ distances (d) in the $B_4X_6:nH_2$ complexes, as gathered in Table 1, three groups can be clearly distinguished: (i) $X = \{CH_2, NH\}$ with d distances of ~ 2.7 Å (ii) $X = \{PH, S\}$ with d distances of ~ 3.0 Å and (iii) $X = O$, with shorter d distances down to ~ 1.6 Å. The case for B_4O_6 is quite remarkable. As more H_2 molecules are attached to B_4O_6 , the $d(B\cdots H_2)$ distances are elongated steadily up to $d \sim 1.85$ Å, and the $H\cdots H$ molecules remain slightly stretched down to $\Delta \sim 0.016$ Å. This behavior for the B_4O_6 systems is unique as compared to the other systems since in the latter the attachment of the H_2 molecules is quite farther to the B atom and the H_2 molecules remain practically unaltered. There is no clear tendency—as compared to B_4O_6 —for the d distances as more H_2 molecules are added for $X = \{CH_2, NH, PH, S\}$, with tiny differences for the series $1 \leq n \leq 4$.

Turning now to the H-H distances in the complexes, as shown in Table 1, in the energy minimum structures of the complexes, the H-H distances are very similar as compared to the isolated H_2 molecule, 0.755 Å. However, there is an exception for the oxygen complexes: when one H_2 molecule is attached to the B_4O_6 system, the $H\cdots H$ bond is elongated by $\Delta \sim 0.02$ Å. As further H_2 molecules are attached to the B_4O_6 system, this elongated H-H bond is shortened consecutively by ~ 0.004 Å, down to 0.763 Å in each H-H molecule of the $B_4O_6:4H_2$ complex, though still 0.008 Å longer than in the isolated H-H molecule.

Finally, we show the computed binding energies of the H_2 molecules for the different complexes $B_4X_6:nH_2$ ($n = 1-4$), as seen in Table 2 and displayed in Figure 5, where we also include the CBS extrapolated values. As expected from the computed MESP and energy profiles in $B_4X_6:H_2$ complexes, the larger binding energy for one H_2 molecule corresponds to the B_4O_6 system, with $\Delta E \sim 29$ kJ/mol ($\Delta E_{\text{CBS}} \sim 22$ kJ/mol). For comparative purposes, the electronic binding energy of the water dimer is $\Delta E[(H_2O)_2] \sim 21$ kJ/mol [51].

Table 2. Binding energies (kJ/mol) in optimized ($B_4X_6:nH_2$) complexes, $X = \{CH_2, NH, PH, O, S\}$ with MP2/aug-cc-pVDZ computations and the MP2 complete basis set (CBS) limit obtained by extrapolation of the HF energies calculated at aug-cc-pV k Z, with $k = D, T$ and Q , following Equations (1)–(3). $\Delta E(1:n)$ for a given X corresponds to the binding energy of the complex $B_4X_6:nH_2$.

X	$\Delta E(1:1)$	$\Delta E(1:2)$	$\Delta E(1:3)$	$\Delta E(1:4)$
	MP2 CBS	MP2 CBS	MP2 CBS	MP2 CBS
CH ₂	−6.6 −2.8	−13.3 −5.4	−20.1 −8.0	−26.8 −10.7
NH	−5.8 −2.5	−12.9 −6.1	−20.0 −9.7	−25.8 −12.2
PH	−6.2 −1.6	−13.3 −3.9	−19.9 −6.1	−26.4 −7.7
O	−28.6 −22.1	−49.5 −37.6	−65.5 −49.1	−79.2 −58.9
S	−7.9 −3.3	−15.8 −6.7	−23.4 −10.1	−31.6 −13.5

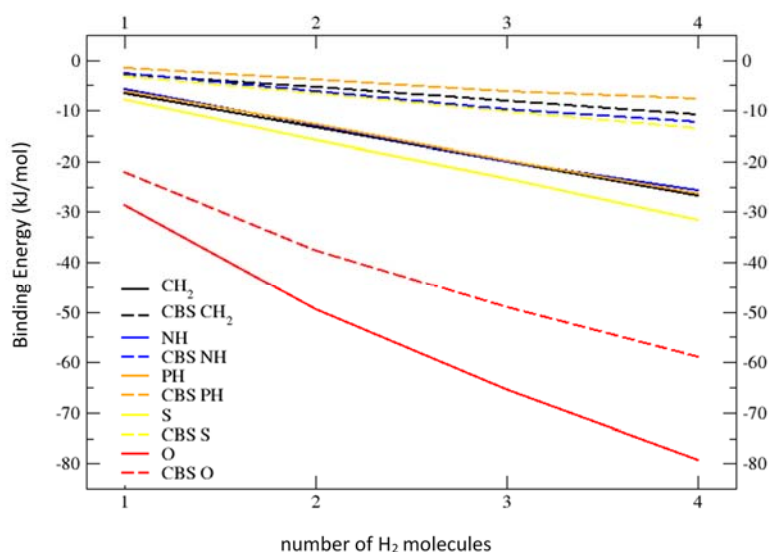


Figure 5. Binding energies of the $B_4X_6:nH_2$ complexes ($n = 1-4$) as function of attached H_2 molecules. MP2/aug-cc-pVDZ computations (solid lines) and extrapolated MP2/CBS limit (dashed lines).

The maximum binding energy for the complexes corresponds to $B_4O_6:4H_2$ with a value of 79 kJ/mol (CBS extrapolation 60 kJ/mol). However, the binding energy of one H_2 molecule attached to the other B_4X_6 systems is remarkably smaller in comparison, especially when the CBS extrapolation is added. The addition of more H_2 molecules to the complexes shows practically additive relations for all X . As displayed in Figure 5, when extrapolated to the CBS limit, we can see several features regarding the binding energies in $B_4X_6:nH_2$ ($n = 1-4$) complexes as compared to the MP2/aug-cc-pVDZ energies: (1) the CBS extrapolated binding energies are smaller for a given X and n (2) the (absolute value of the) slope of ΔE versus n (number of H_2) molecules decreases for CBS extrapolated values (3) both CBS extrapolated and non-extrapolated binding energies follow a similar linear trend, except for $X = O$, the latter with clearly larger (CBS) binding energies, from 20 kJ/mol ($n = 1$) to 60 kJ/mol ($n = 4$).

We should notice that for $X = O$, though the CBS extrapolated slope is smaller than the non-extrapolated one, yet this slope is larger (in absolute value) as compared to the other X s hence the

peculiar behavior of $B_4O_6:nH_2$ as compared to complexes with different Xs. We should also emphasize the small differences (less than ~ 5 kJ/mol) between binding energies for different Xs for a given number n of attached H_2 molecules, with the exception of $X = O$ with larger binding energies.

3. Computational Method

All geometries of the B_4X_6 systems and the corresponding $B_4X_6:nH_2$ ($n = 1-4$) complexes were optimized with second-order Møller-Plesset perturbation theory (MP2) [52] and a double- ζ basis set including polarization and diffuse functions [53], such as aug-cc-pVDZ. The interactions between B_4X_6 systems and H_2 molecules are clearly of noncovalent nature, weaker than conventional chemical bonds, given the closed-shell nature of the species involved and the lack of any further singlet coupling between unpaired electrons. We search for stable complexes $B_4X_6:nH_2$ and dispersive corrections are important given the neutral and spin-zero nature of the involved systems, hence the use of MP2 theory in computations. This theory improves on the Hartree-Fock (a mean-field—molecular-orbital—theory of electronic structure) method by adding electron correlation effects by means of Rayleigh-Schrödinger perturbation theory (RS-PT).

The quantum-chemical computations in this work were carried out at the MP2 level of theory with the scientific software Gaussian09 (Gaussian Inc, Wallingford, CT, USA) [54], and the molecular electrostatic potential (MESP) for the B_4X_6 systems was computed with the DAMQT program [55,56], also at the MP2 level of theory. Frequency computations were performed in order to check the energy minimum nature in all B_4X_6 systems and $B_4X_6:nH_2$ complexes ($n = 1-4$). The binding energies for the $B_4X_6:nH_2$ complexes are computed as $\Delta E = E(B_4X_6:nH_2) - E(B_4X_6) - n \cdot E(H_2)$, and reported in kJ/mol. Further geometry optimizations of all B_4X_6 complexes were carried out with the MP2/aug-cc-pVTZ computational model—with a triple- ζ basis set—in order to check the validity of the optimized geometries (see Supplementary Information). A single-point energy profile (MP2) versus $B \cdots H_2$ distance in the complex $B_4(CH_2)_6:H_2$ was computed using both basis sets: aug-cc-pVDZ and aug-cc-pVTZ (see Supplementary Information), double- ζ and triple- ζ respectively. As shown in Figure S1, the results show similar profiles along the local \hat{C}_3 axis of rotation on the B atom and therefore we can confirm the validity of the MP2/aug-cc-pVDZ computational model for geometries and binding energies.

In order to assess the dependency of the binding energies on basis set incompleteness, we also computed the binding energies of all complexes in the extrapolated complete basis set (CBS) limit. The CBS energy has been calculated by extrapolation of the HF energies calculated at aug-cc-pV k Z, with $k = D, T$ and Q , and Equation (1) and the correlation part with Equation (2). The sum of the two components (HF and correlation) (Equation (3)) provides the MP2(CBS) energy.

$$E_{HF,k} = E_{HF,lim} + Ae^{-Bk} \quad (1)$$

with $k = 2, 3$ and 4 for aug-cc-pVDZ, aug-cc-pVTZ and aug-cc-pVQZ basis sets, respectively [57,58].

$$E_{cor,k} = E_{cor,lim} + Ak^{-3} \quad (2)$$

with $k = 3$ and 4 for aug-cc-pVTZ and aug-cc-pVQZ basis sets, respectively [59]. Finally, we have

$$E_{MP2}(CBS) = E_{HF,lim} + E_{cor,lim} \quad (3)$$

4. Conclusions

From the results obtained in this work we can conclude with the following points:

1) The MESP in the adamantane-like structures B_4X_6 , with $X = \{CH_2, NH, O; SiH_2, PH, S\}$, show π -holes above the B atom with electron (density) attraction forces largest for B_4O_6 and lowest for $B_4(PH)_6$ and B_4S_6 .

2) The energy profiles of one H_2 molecule approaching along a C_{3v} axes the B atom of B_4X_6 systems show attractive patterns up to certain values for all systems where it turns to repulsive below

~ 2.1 Å for B₄(CH₂)₆ and B₄(NH)₆ and below ~ 2.5 Å for B₄(PH)₆ and B₄S₆, except for B₄(SiH₂)₆ where the profile is always attractive with H₂ bond breaking and cage rearrangement. For B₄O₆, there is a flat energy minimum region within 1.7–2.0 Å.

3) The attraction strength for electron density towards boron atoms in B₄X₆ is also shown in the energy profiles of the B₄X₆:H₂ complexes as a function of the B··H₂ distance *d*. The *d* distances in the energy minima structures coincide with the predicted distances from the energy profiles.

4) The binding energies of the B₄X₆:*n*H₂ complexes—*n* = 1–4, follow a similar linear additive pattern (in magnitude and direction) for all X, except X = O, with larger binding energies. CBS extrapolation shows a significant decrease in the binding energies.

Supplementary Materials: The following are available online at <http://www.mdpi.com/1420-3049/25/5/1042/s1>, Figure S1: Plot of ΔE (kJ/mol) versus *d* (Å) for the complex [B₄(CH₂)₆]··H₂ for a range of distances 1.25 Å ≤ *d* ≤ 4.0 Å and a step Δ*d* = 0.25 Å. MP2/aug-cc-pVDZ (red solid line) and MP2/aug-cc-pVTZ (green dashed line) computations, Figure S2: Optimized structures of the B₄X₆:*n*H₂ complexes (*n* = 1–4), X = {CH₂; NH, PH; S} with MP2/aug-cc-pVDZ computations. All geometries correspond to energy minima, Table S1: Cartesian coordinates (Å) of MP2/aug-cc-pVDZ (left column) and MP2/aug-cc-pVTZ (right column) optimized geometries corresponding to energy minima of the adamantane analogue systems B₄X₆ with X = {CH₂, SiH₂; NH, PH; O, S}. All molecules have T_d symmetry except B₄X₆ with X = {NH, PH} which have C₁ symmetry.

Author Contributions: Conceptualization, J.E., I.A. and J.M.O.-E.; methodology, I.A. and J.M.O.-E.; software, I.A. and J.M.O.-E.; validation, I.A. and J.M.O.-E.; formal analysis, I.A. and J.M.O.-E.; investigation, I.A. and J.M.O.-E.; resources, I.A. J.M.O.-E., and J.E.; writing—original draft preparation, J.M.O.-E. and I.A.; writing—review and editing, J.M.O.-E. and I.A.; supervision, J.E., I.A. and J.M.O.-E.; project administration, I.A.; funding acquisition, I.A. and J.E. All authors have read and agreed to the published version of the manuscript.

Funding: We are grateful to Spanish MICINN for financial support through project CTQ2018-094644-B-C22 and Comunidad de Madrid (P2018/EMT-4329 AIRTEC-CM).

Conflicts of Interest: The authors declare no conflict of interest.

References

- Zell, T.; Langer, R. *Hydrogen storage*; Walter de Gruyter: Berlin, Germany, 2019.
- Moradi, R.; Groth, K.M. Hydrogen storage and delivery: Review of the state of the art technologies and risk and reliability analysis. *Int. J. Hydro. Energy* **2019**, *44*, 12254–12269. [[CrossRef](#)]
- Preuster, P.; Alekseev, A.; Wasserscheid, P. Hydrogen storage technologies for future energy systems. *Annu. Rev. Chem. Biomol.* **2017**, *8*, 445–471. [[CrossRef](#)] [[PubMed](#)]
- Mohan, M.; Sharma, V.K.; Kumar, E.A.; Gayathri, V. Hydrogen storage in carbon materials—A review. *Energy Stor.* **2019**, *1*, 1–26. [[CrossRef](#)]
- Khan, N.; Dilshad, S.; Khalid, R.; Kalair, A.R.; Abas, N. Review of energy storage and transportation of energy. *Energy Stor.* **2019**, *1*, 1–49. [[CrossRef](#)]
- Schneemann, A.; White, J.L.; Kang, S.; Jeong, S.; Wan, L.F.; Cho, E.S.; Heo, T.W.; Prendergast, D.; Urban, J.J.; Wood, B.C.; et al. Nanostructured metal hydrides for hydrogen storage. *Chem. Rev.* **2018**, *118*, 10775–10839. [[CrossRef](#)] [[PubMed](#)]
- Suh, M.P.; Park, H.J.; Prasad, T.K.; Lim, D.-W. Hydrogen storage in metal-organic frameworks. *Chem. Rev.* **2012**, *112*, 782–835. [[CrossRef](#)]
- Kapelewski, M.T.; Runčevski, T.; Tarver, J.D.; Jiang, H.Z.H.; Hurst, K.E.; Parilla, P.A.; Ayala, A.; Gennett, T.; Fitzgerald, S.A.; Brown, C.M.; et al. Record High Hydrogen Storage Capacity in the Metal–Organic Framework Ni₂(m-dobdc) at Near-Ambient Temperatures. *Chem. Mater.* **2018**, *30*, 8179–8189. [[CrossRef](#)]
- Zhu, B.; Zou, R.; Xu, Q. Metal–organic framework based catalysts for hydrogen evolution. *Adv. Energy Mater.* **2018**, *8*, 1801193. [[CrossRef](#)]
- Yan, Y.; da Silva, I.; Blake, A.J.; Dailly, A.; Manuel, P.; Yang, S.; Schröder, M. High volumetric hydrogen adsorption in a porous anthracene-decorated metal–organic framework. *Inorg Chem.* **2018**, *57*, 12050–12055. [[CrossRef](#)]
- Koizumi, K.; Nobusada, K.; Boero, M. Hydrogen storage mechanism and diffusion in metal–organic frameworks. *Phys. Chem. Chem. Phys.* **2019**, *21*, 7756–7764. [[CrossRef](#)]
- Hobza, P.; Müller-Dethlefs, K. *Non-Covalent Interactions. Theory and Experiment*; Royal Society of Chemistry: Cambridge, UK, 2009.

13. Chakraborty, A.; Giri, S.; Chattaraj, P.K. Analyzing the efficiency of $M_n-(C_2H_4)$ ($M = Sc, Ti, Fe, Ni; n = 1, 2$) complexes as effective hydrogen storage materials. *Struct. Chem.* **2011**, *22*, 823–837. [CrossRef]
14. Ma, L.-J.; Jia, J.; Wu, H.-S. Computational investigation of hydrogen storage on scandium–acetylene system. *Int. J. Hydro. Energy* **2015**, *40*, 420–428. [CrossRef]
15. Konda, R.; Titus, E.; Chaudhari, A. Adsorption of molecular hydrogen on inorganometallic complexes B_2H_4M ($M = Li, Be, Sc, Ti, V$). *Struct. Chem.* **2018**, *29*, 1593–1599. [CrossRef]
16. Konda, R.; Kalamse, V.; Deshmukh, A.; Chaudhari, A. Closoborate-transition metal complexes for hydrogen storage. *RSC Adv.* **2015**, *5*, 99207–99216. [CrossRef]
17. Naumkin, F.Y.; Wales, D.J. Hydrogen trapped in Be_n cluster cages: The atomic encapsulation option. *Chem. Phys. Lett.* **2012**, *545*, 44–49. [CrossRef]
18. Meng, Y.; Han, Y.; Zhu, H.; Yang, Z.; Shen, K.; Suo, B.; Lei, Y.; Zhai, G.; Wen, Z. Two dimetalloenes with vanadium and chromium: Electronic structures and their promising application in hydrogen storage. *Int. J. Hydro. Energy* **2015**, *40*, 12047–12056. [CrossRef]
19. Grabowski, S.; Ruiperez, F. Dihydrogen bond interactions as a result of H_2 cleavage at Cu, Ag and Au centres. *Phys. Chem. Chem. Phys.* **2016**, *18*, 12810–12818. [CrossRef]
20. Alkorta, I.; Elguero, J.; Solimannejad, M.; Grabowski, S.J. Dihydrogen bonding vs metal– σ interaction in complexes between H_2 and metal hydride. *J. Phys. Chem. A* **2011**, *115*, 201–210. [CrossRef]
21. Alkorta, I.; Montero-Campillo, M.M.; Elguero, J.; Yáñez, M.; Mó, O. Complexes between H_2 and neutral oxyacid beryllium derivatives. The role of angular strain. *Mol. Phys.* **2019**, *117*, 1142–1150. [CrossRef]
22. Alkorta, I.; Montero-Campillo, M.M.; Elguero, J.; Yáñez, M.; Mó, O. Complexes between neutral oxyacid beryllium salts and dihydrogen: A possible way for hydrogen storage? *Dalton Trans.* **2018**, *47*, 12516–12520. [CrossRef]
23. Kayal, S.; Manna, U.; Das, G. Steric influence of adamantane substitution in tris-urea receptor: Encapsulation of sulphate and fluoride-water cluster. *J. Chem. Sci.* **2018**, *130*, 1–6. [CrossRef]
24. Hooley, R.J.; Shenoy, S.R.; Rebek, J., Jr. Electronic and steric effects in binding of deep cavitands. *Org. Lett.* **2008**, *10*, 5397–5400. [CrossRef] [PubMed]
25. Wanka, L.; Iqbal, K.; Schreiner, P.R. The lipophilic bullet hits the targets: Medicinal chemistry of adamantane derivatives. *Chem. Rev.* **2013**, *113*, 3516–3604. [CrossRef] [PubMed]
26. Fort, R.C. *Adamantane: The chemistry of diamond molecules*; Marcel Dekker: New York, NY, USA, 1976.
27. Spilovska, K.; Zemek, F.; Korabecny, J.; Nepovimova, E.; Soukup, O.; Windisch, M.; Kuca, K. Adamantane – A lead structure for drugs in clinical practice. *Curr. Med. Chem.* **2016**, *23*, 3245–3266. [CrossRef]
28. Schwertfeger, H.; Fokin, A.A.; Schreiner, P.R. Diamonds are a chemist’s best friend: Diamondoid chemistry beyond adamantane. *Angew. Chem. Int. Ed.* **2008**, *47*, 1022–1036. [CrossRef]
29. Bagrii, E.I.; Nekhaev, A.I.; Maksimov, A.L. Oxidative functionalization of adamantanes. *Petrol. Chem.* **2017**, *57*, 183–197. [CrossRef]
30. Štimac, A.; Šekutor, M.; Mlinarić-Majerski, K.; Frkanec, L.; Frkanec, R. Adamantane in drug delivery systems and surface recognition. *Molecules* **2017**, *22*, 297. [CrossRef]
31. Speckamp, W.N.; Dijkink, J.; Huisman, H.O. 1-Aza-adamantanes. *J. Chem. Soc. D: Chem. Comm.* **1970**, *4*, 197–198. [CrossRef]
32. Shibuya, M.; Tomizawa, M.; Suzuki, I.; Iwabuchi, Y. 2-Azaadamantane N-Oxyl (AZADO) and 1-Me-AZADO: highly efficient organocatalysts for oxidation of alcohols. *J. Am. Chem. Soc.* **2006**, *128*, 8412–8413. [CrossRef]
33. Kirillo, A.M. Hexamethylenetetramine: An old new building block for design of coordination polymers. *Coordin. Chem. Rev.* **2011**, *255*, 1603–1622. [CrossRef]
34. Dreyfors, J.M.; Jones, S.B.; Sayed, Y. Hexamethylenetetramine: A review. *Am. Ind. Hyg. Assoc. J.* **1989**, *50*, 579–585. [CrossRef] [PubMed]
35. Bane, V.; Lehane, M.; Dikshit, M.; O’Riordan, A.; Furey, A. Tetrodotoxin: Chemistry, toxicity, source, distribution and detection. *Toxins* **2014**, *6*, 693–755. [CrossRef] [PubMed]
36. Mancini, I.; Guella, G.; Frostin, M.; Hnawia, E.; Laurent, D.; Debitus, C.; Pietra, F. On the first polyarsenic organic compound from Nature: Arsenicin A from the new caledonian marine sponge echinochalina bargibanti. *Chem. Eur. J.* **2006**, *12*, 8989–8994. [CrossRef]
37. Whitlow, K.S.; Belson, M.; Barrueto, F.; Nelson, L.; Henderson, A.K. Tetramethylenedisulfotetramine: Old agent and new terror. *Ann. Emerg. Med.* **2005**, *45*, 609–613. [CrossRef] [PubMed]
38. Available online: https://en.wikipedia.org/wiki/Phosphorus_pentasulfide (accessed on 12 December 2019).

39. Shi, Y.X.; Xu, K.; Clegg, J.K.; Ganguly, R.; Hirao, H.; Friščić, T.; García, F. The first synthesis of the sterically encumbered adamantoid phosphazane $P_4(NtBu)_6$: Enabled by mechanochemistry. *Angew. Chem. Int. Ed.* **2016**, *55*, 12736–12740. [[CrossRef](#)] [[PubMed](#)]
40. Kutsumura, N.; Ohshita, R.; Horiuchi, J.; Tateno, K.; Yamamoto, N.; Saitoh, T.; Nagumo, Y.; Kawai, H.; Nagase, H. Synthesis of heterocyclic compounds with adamantane-like cage structures consisting of phosphorus, sulfur, and carbon. *Tetrahedron* **2017**, *73*, 5214–5219. [[CrossRef](#)]
41. Mikhailov, B.M. Reactions of allylboranes with unsaturated compounds. *Pure Appl. Chem.* **1980**, *52*, 691–704. [[CrossRef](#)]
42. El-Hamdi, M.; Solà, M.; Poater, J.; Timoshkin, A.Y. Complexes of adamantane-based group 13 Lewis acids and superacids: Bonding analysis and thermodynamics of hydrogen splitting. *J. Comput. Chem.* **2016**, *37*, 1355–1362. [[CrossRef](#)]
43. García, J.C.; Justo, J.F.; Machado, W.V.M.; Assali, L.V.C. Functionalized adamantane: Building blocks for nanostructure self-assembly. *Phys. Rev. B* **2009**, *80*, 125421. [[CrossRef](#)]
44. Murray, J.S.; Lane, P.; Politzer, P. A predicted new type of directional noncovalent interaction. *Int. J. Quantum Chem.* **2007**, *107*, 2286–2292. [[CrossRef](#)]
45. Mohajeri, A.; Pakiari, A.H.; Bagheri, N. Theoretical studies on the nature of bonding in σ -hole complexes. *Chem. Phys. Lett.* **2009**, *467*, 393–397. [[CrossRef](#)]
46. Politzer, P.; Murray, J.; Concha, M. σ -hole bonding between like atoms; a fallacy of atomic charges. *J. Mol. Model.* **2008**, *14*, 659–665. [[CrossRef](#)] [[PubMed](#)]
47. Sánchez-Sanz, G.; Trujillo, C.; Solimannejad, M.; Alkorta, I.; Elguero, J. Orthogonal interactions between nitril derivatives and electron donors: Pnictogen bonds. *Phys. Chem. Chem. Phys.* **2013**, *15*, 14310–14318. [[CrossRef](#)] [[PubMed](#)]
48. Solimannejad, M.; Ramezani, V.; Trujillo, C.; Alkorta, I.; Sánchez-Sanz, G.; Elguero, J. Competition and interplay between σ -hole and π -hole interactions: A computational study of 1:1 and 1:2 complexes of nitril halides (O_2NX) with ammonia. *J. Phys. Chem. A* **2012**, *116*, 5199–5206. [[CrossRef](#)] [[PubMed](#)]
49. Murray, J.; Lane, P.; Clark, T.; Riley, K.; Politzer, P. σ -holes, π -holes and electrostatically-driven interactions. *J. Mol. Model.* **2012**, *18*, 541–548. [[CrossRef](#)]
50. Saida, A.B.; Chardon, A.; Osi, A.; Tumanov, N.; Wouters, J.; Adjieufack, A.I.; Champagne, B.; Berionni, G. Pushing the Lewis acidity boundaries of boron compounds with non-planar triarylboranes derived from triptycenes. *Angew. Chem. Int. Ed.* **2019**, *58*, 1–6.
51. Feyereisen, M.W.; Feller, D.; Dixon, D.A. Hydrogen bond energy of the water dimer. *J. Phys. Chem.* **1996**, *100*, 2993–2997. [[CrossRef](#)]
52. Møller, C.; Plesset, M.S. Note on an approximation treatment for many-electron systems. *Phys. Rev.* **1934**, *46*, 618–622. [[CrossRef](#)]
53. Kendall, R.A.; Dunning, T.H., Jr.; Harrison, R.J. Electron affinities of the first-row atoms revisited. Systematic basis sets and wave functions. *J. Chem. Phys.* **1992**, *96*, 6796–6806. [[CrossRef](#)]
54. *Gaussian 09, Revision, E.01*; Gaussian Inc.: Wallingford, CT, USA, 2019.
55. Kumar, A.; Yeole, S.D.; Gadre, S.R.; López, R.; Rico, J.F.; Ramirez, G.; Ema, I.; Zorrilla, D. DAMQT 2.1.0: A new version of the DAMQT package enabled with the topographical analysis of electron density and electrostatic potential in molecules. *J. Comput. Chem.* **2015**, *36*, 2350–2359. [[CrossRef](#)]
56. López, R.; Fernández Rico, J.; Ramírez, G.; Ema, I.; Zorrilla, D. DAMQT: A package for the analysis of electron density in molecules. *Comput. Phys. Commun.* **2009**, *180*, 1654–1660. [[CrossRef](#)]
57. Feller, D. The use of systematic sequences of wave functions for estimating the complete basis set, full configuration interaction limit in water. *J. Chem. Phys.* **1993**, *98*, 7059. [[CrossRef](#)]
58. Williams, T.G.; DeYonker, N.J.; Wilson, A.K. Hartree-Fock complete basis set limit properties for transition metal diatomics. *J. Chem. Phys.* **2008**, *128*, 044101. [[CrossRef](#)] [[PubMed](#)]
59. Halkier, A.; Helgaker, T.; Jorgensen, P.; Klopper, W.; Olsen, J. Basis-set convergence of the energy in molecular Hartree-Fock calculations. *Chem. Phys. Lett.* **1999**, *302*, 437–446. [[CrossRef](#)]

